POS-A-40

3D PATTERN MEASUREMENT OF LOG-PERIODIC DIPOLE ANTENNAT USING PHOTONIC SENSOR AND SPHERICAL NEAR-FIELD SCANNING BELOW 2 GHZ

Masanobu HIROSE, Satoru KUROKAWA, and Koji KOMIYAMA
National Metrology Institute of Japan, AIST
1-1-1, Umezono, Tsukuba-shi, Ibaraki, 305-8568, Japan
masa-hirose@aist.go.jp

Takauki ISHIZONE
Dept. of Electrical and Electronic Engineering, Toyo University
Kujirai 2100, Kawagoe, Saitama 350-8585, Japan

1. Introduction

The spherical near-field measurement method (SNM) [1] is a technique to measure antenna patterns of broad beamwidth antennas. Conventionally, an open-ended waveguide (OEW) is used as a probe of the SNM. The OEW is made of metal bulk and the aperture is as large as a half-wavelength. Then the scanning equipment becomes heavy and large at frequency below about 2 GHz. Conversely, a system using a photonic sensor as the probe can be compact because the sensor is small (a few mm) and light (a grams). Therefore the system using the photonic sensor can be a promising system of the SNM below about 2 GHz as well as of the planar near-field measurement method for directive antennas [2].

To demonstrate the usefulness of the photonic sensor in the SNM below 2 GHz, we have measured the near field of the log-periodic dipole antenna (LPDA) that is often used in EMC (Electromagnetic compatibility) measurements and has broad pattern.

Comparing the measured patterns with the ones measured by the conventional far-field method and the ones calculated by FDTD, we have found that the patterns agree within about 2dB in the broad main beams. Therefore the photonic sensor can be used as a probe for the near-field measurements below 2 GHz and can be considered as an infinitesimal electric dipole antenna.

2. Photonic sensor

In the previous paper [2], we explained the operation principle and the structure of the photonic sensor in detail. The sensor is slightly different form the one that we used in this paper. However its characteristics are almost the same. The basic structure of the sensor is a type of Mach-Zehnder interferometer. The geometrical structure is shown in Fig. 1. The $LiNbO_3$ substrate is of 3 mm width, 0.5 mm thickness, and 8 mm length. The antenna is a rectangular dipole antenna whose total length is 2.4 mm and its base width is 2 mm. Since a small mirror is made at the left side in Fig. 1, the sensor is called as a reflection type. Because it consists of dielectric materials except the metallic antenna and their sizes are very small compared to the wavelength (0.016 wavelength at 2 GHz), the sensor can be considered to be an infinitesimal electric dipole antenna that does not disturb the original electromagnetic field to be measured.

The basic operation principle is as follows. External electric field excites voltage between the center of the dipole antenna on the sensor. The voltage modulates the amplitude of the laser beam simultaneously. Then, detecting its amplitude electrically, we can measure the external electric field simultaneously.

3. Measurement setup for the photonic sensor and spherical scanning

As measurement equipment, we use a spherical scanning system that consists of two rotators as in Fig. 2. The one is uses as the phi rotation and has the foam polystyrene block on it to support the LPDA. The other is used as the theta rotation and has the structure to support the photonic sensor. The measurement view is shown in Fig. 3. The LPDA is Schwarzbeck's UHALP9108A1 in Fig. 4, which is often used from 250 MHz to 2400 MHz in EMC measurements. Electromagnetic absorbers are fixed to the structure. The sensor is fixed on the top of a glass pipe that is fixed to the structure. The locus of

the sensor is on the circle whose radius is 0.55 m and angle is from 0 degree to 159 degrees. The center of the circle corresponds to the coordinate origin. The top of the LPDA is set at r=0.42 m and rotated around the z-axis (the vertical axis in Fig. 2) form 0 degree to 357 degrees by 3 degrees. The vector network analyzer (VNA) was Agilent E8364A whose IF bandwidth and power were 10 Hz and -11 dBm respectively. A power amplifier of 25 dB was connected to the output port of the VNA to increase the sensitivity of the measurement system. The measured SNR was about 40 dB.

4. Near- to Far-field transformation

In Ref. [2], we have shown that the photonic sensor can be considered to be an infinitesimal electric antenna with a linear polarization. As shown by Kerns [2, 3], S_{21} between an AUT and an infinitesimal electric antenna with a linear polarization is proportional to the inner product of the electric field E created by the AUT and the electric moment vector p as

$$S_{21} = const. \, E(r) \bullet p \tag{1}.$$

If p is parallel to the theta or phi directions, S_{21} is proportional to the corresponding component of the electric field. The polarization vector is parallel to the electric moment vector p of the antenna on the photonic sensor. Therefore we can measure the theta and phi components of the electric field using the photonic sensor on a sphere by the spherical scanning system.

To obtain the far-field patterns, the coefficients for the TE and TM waves in the spherical wave functions were determined by Ludwig's method using the measured S_{21}s that are proportional to the theta and phi components of the electric field due to Eq. (1) [1]. Using the coefficients, the far-field pattern is calculated by transforming the TE and TM waves into the far-field expressions. We stress here that we can calculate the far-field pattern without probe correction when using the photonic sensor.

5. Antenna patterns

Figure 5 shows the measured electric near-field components using the photonic sensor at 1 GHz. E.co (H.co) and E.cross (H.cross) mean the copolar and cross-polar components in the E (H) plane respectively. The definitions of the polarization follow the Ludwig's 3rd definition [1]. Transforming the near-field data to the far-field pattern, we obtained the copolar patterns of the E and H plane in Fig.6 and the cross-polar patterns in Fig. 7. Comparing Fig. 5, Fig. 6, and Fig.7, we can find that the near-field are quite different from the far-field patterns because the radiation center of the LPDA is eccentric to the center of the theta rotation and the distance between the LPDA and the photonic sensor is close.

In Fig. 6 and 7, we also show the results calculated by XFDTD [4] and the ones measured by the conventional far-field method. XFDTD is a commercially available FDTD software. In the calculation by XFDTD, we divide the calculation space of 980 m x 940 mm x 400 mm into 490 x 470 x 200 cells with the grid size of 2.0 mm and the time step of 3.85 ps. The Liao absorption boundary condition is used.

In Fig. 6, the copolar patterns by XFDTD and the far-field method agree well with each other and the ones by the photonic sensor are broader. We infer from the disagreement of the H.cross and E.cross components at the point where theta = 0 degrees in Fig. 5 that the two electric moment p of the sensor are not orthogonal to each other. We also infer that the locus of the sensor is not on the sphere because the mechanical strength of the scanning system was not sufficient. In Fig. 7, the cross-polar patterns by the three methods are different. Since the model used by XFDTD does not include a rod to support the whole LPDA in Fig. 4, the absence of the rod can affect the low-level patterns. The position errors of the photonic sensor also deteriorate the antenna patterns. However the levels of the patterns are around –20 dB.

We show the copolar far-field patterns at 2 GHz in Fig. 8. The agreement of the patterns by the three methods is better than those at 1 GHz. We infer it from the reason that the radial component of the electric field does not affect the measured tangential components due to the direction error of the photonic sensor because the scanning radius normalized to the wavelength becomes large and the radial component becomes small.

Using the spherical near-field measurement method, we can measure the 3D antenna patterns.

As an example, we show the 3D patterns of the copolar and cross-polar components at 1 GHz. From Fig. 10, we can find that there are the areas where the cross-polar component becomes about –10 dB.

6. Conclusions

We have developed the spherical near-field scanning equipment using a photonic sensor as the probe and measured the 3D far-field patterns below 2 GHz. The patterns agree with the ones measured by the conventional far-field method and calculated by FDTD within about 2 dB in the main beam.

Considering the results in this paper and the previous paper [2], we have demonstrated that the photonic sensor can be used as a broadband probe in the near-field measurements below about 10 GHz. That is, we can measure the 3D far-field patterns combined with near-field measurement methods and the only one photonic sensor; we need not change the probe depending on the measurement frequencies as we do using the conventional probes.

To decrease the measurement errors (or uncertainties), we have a plan to build a new spherical scanning equipment whose position and direction errors are negligible. In the near future, we will determine the uncertainties of the measurements using the photonic sensor combined with the near-field measurement methods.

References
[1] J. E. Hansen ed., *Spherical Near-Field Antenna Measurements*, IEE Electromagnetic waves series 26, 1988.
[2] M. Hirose, T. Ishizone, and K. Komiyama, "Antenna Pattern Measurements Using Photonic Sensor for Planar Near-Field Measurement at X Band", accepted and appears on March 2004 in IEICE Trans. Communications.
[3] D. M. Kerns, *Plane-Wave Scattering-Matrix Theory of Antennas and Antenna-Antenna Interactions*, NBS Monograph 162, 1981.
[4] Remcom Inc., *User's Manual for XFDTD the Finite Difference Time Domain Graphical User Interface for Electromagnetic Calculations*, Version 5.0, 133pp, 1998.
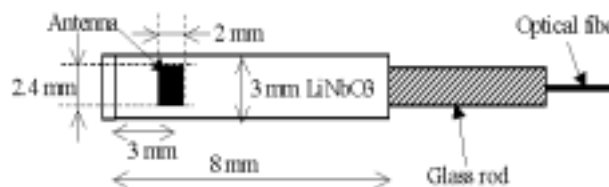
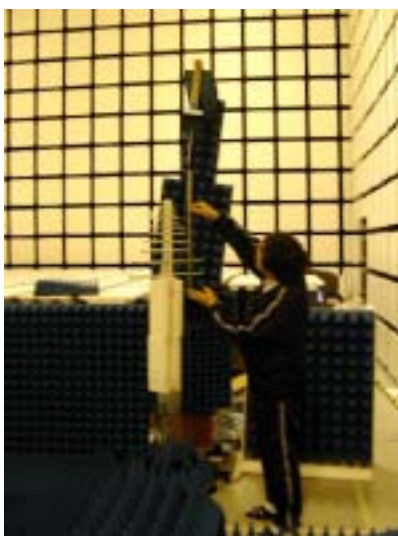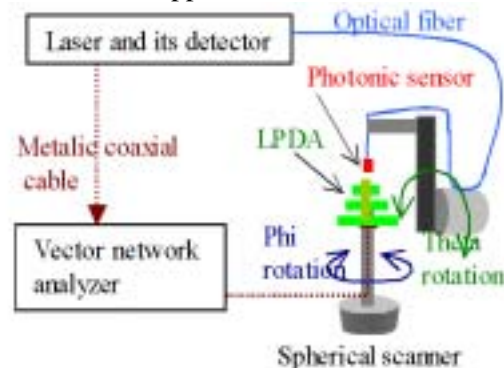Fig. 1 Geometrical structure of the photonic sensor.

Fig.2 Measurement setup.

Fig.3 Measurement view.

Fig. 4 Picture of the LPDA. The L-angled scale is 50 cm x 25 cm long.
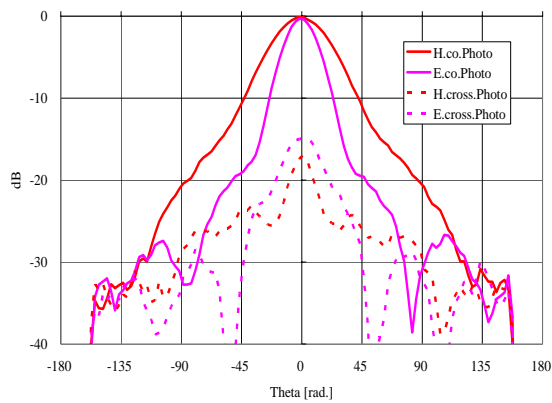
Fig. 5 Measured electric near-field components in the H and E plane of the LPDA at 1 GHz.
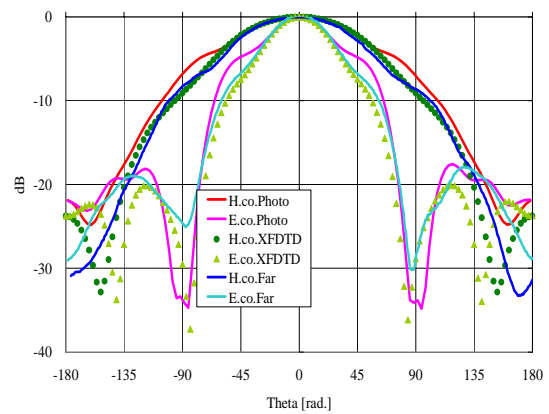

Fig. 6 Comparison of the copolar patterns in the H and E plane of the LPDA at 1 GHz. The subscripts, Photo, XFDTD, and Far indicate the results by each method.
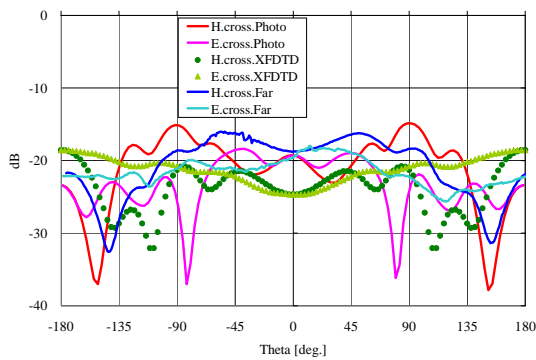

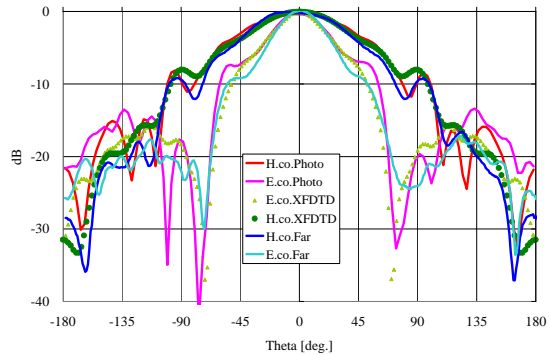Fig. 7 Comparison of the cross-polar patterns in the H and E plane of the LPDA at 1 GHz.

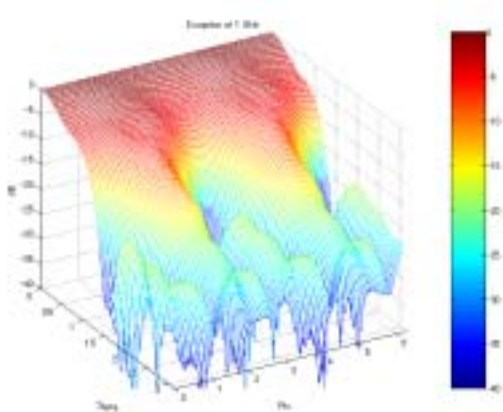Fig. 8 Comparison of the copolar patterns in the H and E plane of the LPDA at 2 GHz.

Fig. 9 3D copolar pattern of the LPDA obtained by the photonic sensor at 1 GHz. Colorbar is from -40 dB to 0 dB by 5 dB.
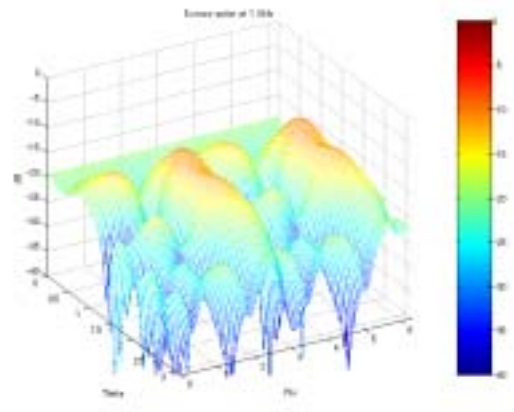

Fig. 10 3D cross-polar pattern of the LPDA obtained by the photonic sensor at 1 GHz. Colorbar is from -40 dB to 0 dB by 5 dB.